Cooperative processes and upconversion in Cs_2NaYCl_6 codoped with Os^{4+} and Er^{3+}

Markus Wermuth, Andrea Schmitz, and Hans U. Güdel
Department of Chemistry and Biochemistry, University of Bern, Frelestrasse 3, CH-3012 Bern, Switzerland
(Received 22 December 2000; revised manuscript received 28 March 2001; published 7 June 2001)

Halide lattices singly doped with Os^{4+} or Er^{3+} are both known to show visible upconversion luminescence upon excitation around 10 000 cm^{-1}. In this study, we analyze the cooperative processes in Cs_2NaYCl_6 codoped with Os^{4+} and Er^{3+} by measuring luminescence intensities and lifetimes. The excitation energy is found to be transferred from the $\Gamma_5(^1T_{2g})/\Gamma_3(^1E_g)$ states of Os^{4+} to $^4I_{11/2}$ and $^4I_{13/2}$ of Er^{3+}. These initial steps are followed by upconversion processes leading to Er^{3+} $^4S_{3/2}$ upconversion emission. The upconversion efficiency upon excitation into $\Gamma_5(^1T_{2g})/\Gamma_3(^1E_g)$ of Os^{4+} critically depends on the Er^{3+} concentration, and among the Cs_2NaYCl_6:x%Er^{3+}, 0.1% Os^{4+} ($x=2$, 10, and 100) samples it is highest for $x=10$. The overall upconversion efficiency is limited by backtransfer processes from the Er^{3+} $^4I_{11/2}$ and $^4S_{3/2}$ states to Os^{4+} and by the low Os^{4+} concentration. An upconversion-excitation mode for Er^{3+} at the energy of the $^4I_{13/2}\rightarrow{}^4S_{3/2}$ excited-state absorption is observed for the title compound.

DOI: 10.1103/PhysRevB.63.245118 PACS number(s): 78.55.Hx, 78.47.+p

I. INTRODUCTION

Upconversion, i.e., photoexcitation at a long wavelength followed by luminescence at a shorter wavelength, is common in compounds containing rare-earth ions.[1] Several upconversion mechanisms are well established in $4f$ systems. Common to all of them is a long-lived intermediate state that acts to store the excitation energy. From this intermediate state, the excitation can be upconverted either radiatively by excited-state absorption (ESA) or nonradiatively by energy transfer with a neighboring excited ion. A limiting factor in the upconversion efficiency of rare-earth ion systems is the small cross section of the f-f absorptions. Sensitization is therefore a common procedure to improve the efficiency of upconverting materials.

The most frequently used sensitizer is Yb^{3+}.[1] Its f^{13}-electron configuration leads to only one f-f excited multiplet located slightly above 10 000 cm^{-1}. Yb^{3+} is thus ideally suited to act as a sensitizer for Pr^{3+},[2] Ho^{3+},[3] Er^{3+},[4] and Tm^{3+}.[5] Above 11 000 cm^{-1}, Yb^{3+} is transparent, and consequently does not interfere with the upconversion luminescence of the activator. The disadvantages of Yb^{3+} regarding its sensitization potential relate to the properties arising from the f-f character of the Yb^{3+} $^2F_{7/2}\rightarrow{}^2F_{5/2}$ transition: The absorption is weak, spectrally narrow, and can barely be chemically tuned.

Absorption intensities of spin-allowed transitions of $3d$ transition-metal ion compounds are larger than those observed in f-f transitions, and, due to the stronger dependence of the energetic positions of d-d excited states on the ligand field, transition-metal ions offer a larger chemical tuning potential compared to lanthanides. The poorly shielded d electrons promise a strong interaction of $3d$ transition-metal sensitizers with potential activators. From this point of view, $3d$ transition-metal ions appear to be ideal sensitizers for rare-earth ion upconversion. However, these advantageous properties are intrinsically coupled with one major drawback: The broad spin-allowed d-d absorption bands of $3d$ transition-metal ions usually cover a considerable part of the visible spectral range, and therefore back-transfer of the upconverted population to the transition-metal sensitizer is very likely. This is the reason why the field of transition-metal ion sensitization of upconversion systems is still largely unexplored.

The situation looks more favorable for $4d$ and $5d$ transition-metal ions, that are known to experience very strong ligand fields. Their broad spin-allowed d-d transitions are consequently found at high energies, and, apart from spectrally narrow spin-flip transitions that can be used as pumping levels, the visible spectral range is empty. Indeed, the only examples of transition-metal ion sensitization of rare-earth ion upconversion described in the literature take advantage of these favorable properties. They reported on Re^{4+} and Mo^{3+} sensitizing Tm^{3+} upconversion.[6–8]

Unfortunately, the absorption intensities of spin-flip transitions are significantly lower than those of spin-allowed d-d transitions, and their energies depend only weakly on the environment via the covalency dependence of the interelectronic repulsion. With respect to absorption intensities and the chemical tuning potential, the spin-flip excited states of transition-metal ions thus occupy an intermediate position between the f-f transitions of rare-earth ions and the broad spin-allowed d-d transitions of transition-metal ions.

In the following, we describe the cooperative processes between the $5d$ transition-metal ion Os^{4+} and the rare-earth ion Er^{3+} codoped into the cubic elpasolite host Cs_2NaYCl_6. The relevant energy levels of the two ions are shown in Fig. 1. The $5d^4$ electron configuration of Os^{4+} is known to give rise to several metastable excited states, and upconversion in Os^{4+}-doped cubic halide lattices was recently demonstrated.[9–11] The $\Gamma_5(^1T_{2g})/\Gamma_3(^1E_g)$ spin-flip excited states of Os^{4+} around 11 000 cm^{-1} serve as pumping levels for the laser excitation. With the exception of $\Gamma_1(^1A_{1g})$, Os^{4+}-doped chloride lattices are transparent between 12 000 and 20 000 cm^{-1}. Thus Os^{4+} meets the conditions for sensitizing Er^{3+}, which is known to show green $^4S_{3/2}$ upconversion luminescence in many systems after excitation into $^4I_{11/2}$ around 10 000 cm^{-1}. By measuring lumi-

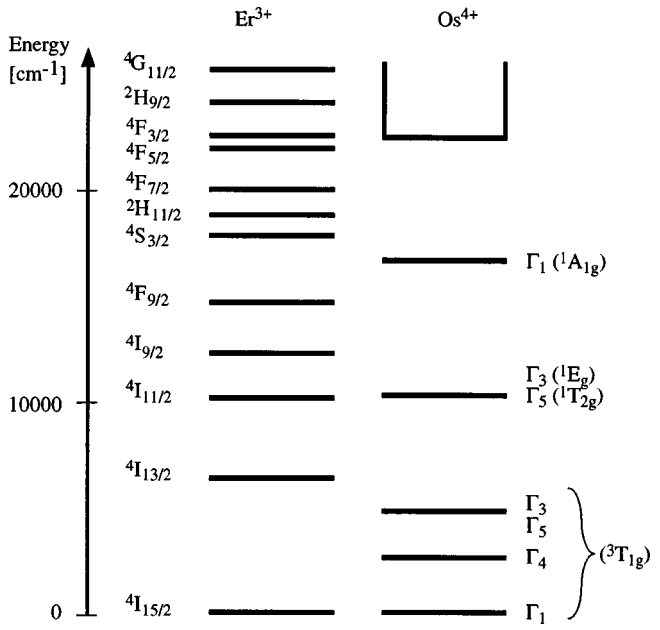

FIG. 1. Energy-level schemes of Er^{3+} and Os^{4+} doped into Cs_2NaYCl_6.

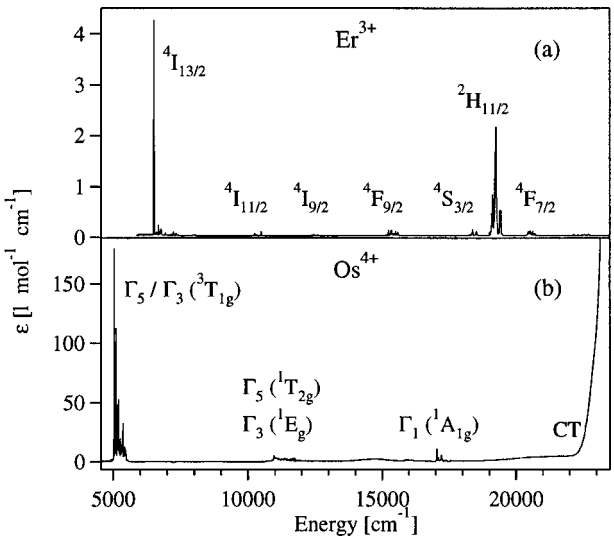

FIG. 2. 15-K absorption spectra of $Cs_2NaYCl_6:Er^{3+}$ (a) and $Cs_2NaYCl_6:Os^{4+}$ (b) in the NIR and VIS (visible) spectral ranges. CT labels the onset of the first charge-transfer band.

nescence intensities and lifetimes in crystals doped with various concentrations of Os^{4+} and Er^{3+}, we elucidate the upconversion mechanisms and investigate the energy-transfer efficiencies.

II. EXPERIMENT

A. Synthesis and crystal growth

Cs_2OsCl_6 was prepared from OsO_4 (99.9%) by reduction with HCl (37%), followed by precipitation with CsCl.[12] The orange product was dried under vacuum. YCl_3 and $ErCl_3$ were prepared from the corresponding oxides (>99.99%) following the ammonium-halide route.[13,14] Using stoichiometric amounts of CsCl, NaCl, YCl_3, $ErCl_3$, and Cs_2OsCl_6, crystals of $Cs_2NaYCl_6:x\%\ Er^{3+},y\%\ Os^{4+}$ ($x=0$, 2, 10, and 100; $y=0$ and 0.1) were grown in silica ampoules by the Bridgman technique. The resulting crystals were cut with a diamond saw, and the surfaces polished. The actual Os^{4+} concentration in the crystal was determined with inductively coupled plasma mass spectrometry and found to be 0.1% even though a nominal concentration of 2% was used. The effective Er^{3+} concentration was assumed to be identical to the nominal Er^{3+} concentration. All handling of the starting material and the resulting crystals was carried out under nitrogen.

B. Spectroscopic measurements

The samples were either enclosed in a copper cell or sealed in silica ampoules, filled with 400-mbar helium for heat dissipation. Cooling was achieved with a closed-cycle cryostat (Air Products) for absorption measurements, or with the helium-gas flow technique for luminescence experiments.

Absorption spectra were recorded on a Cary 5e (Varian). Upconversion-luminescence spectra were obtained using an argon-ion laser (Spectra Physics 2060-10 SA) pumped Ti:sapphire laser (Spectra Physics 3900 S). Wavelength control was achieved by an inchworm driven (Burleigh PZ 501) birefringent filter. The laser beam was focused ($f=50$ mm) on the crystal. The sample luminescence was dispersed by a 0.85-m double monochromator (Spex 1402) or a 0.75-m single monochromator (Spex 1702), and detected by a cooled photomultiplier tube (Hamamatsu 3310-01), using a photon-counting system (Stanford Research 400) or by a liquid-nitrogen-cooled germanium photodiode (ADC 403 L), using a lock-in amplifier (Stanford Research 830). For the lifetime determination of $\Gamma_1(^1A_{1g})$, a dye laser (Lambda Physik FL 3002, Rhodamine 6G in methanol) pumped with the frequency doubled output of a Nd:YAG (yttrium aluminum garnet) laser (Quanta Ray DCR 3, 20 Hz) was used as the excitation source. The luminescence was dispersed and detected as described above and recorded with a multichannel scaler (SR 430). The lifetime of $^4S_{3/2}$ was determined after pulsed excitation with the anti-Stokes Raman-shifted output of the dye laser (Pyridine 1 in methanol). The luminescence decays of $^4I_{11/2}$ and $\Gamma_5(^1T_{2g})/\Gamma_3(^1E_g)$ were determined after excitation with rectangular pulses generated by passing the Ti:sapphire laser beam through an acousto-optic modulator (Coherent 305), connected to a synthesized function generator (Stanford Research DS 345).

Luminescence spectra are corrected for the sensitivity of the detection systems, and displayed as photon counts versus energy. The data were analyzed using Igor (Wave Metrics).

III. RESULTS

All spectra presented in the following were measured at 15 K. Figures 2(a) and 2(b) show the 15-K absorption spectra of Cs_2NaYCl_6:10% Er^{3+} and Cs_2NaYCl_6:0.1% Os^{4+}, respectively. The assignment of the sharp multiplets in the Cs_2NaYCl_6:10% Er^{3+} spectrum is straightforward from a comparison with the literature.[15] The three groups of lines

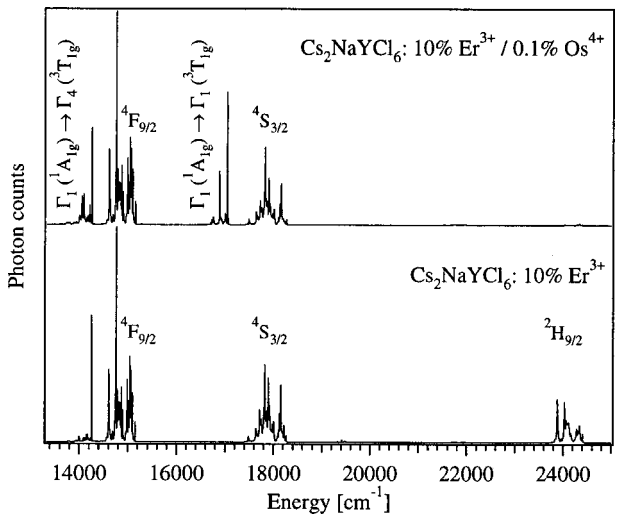

FIG. 3. 15-K upconversion-luminescence spectra of Cs_2NaYCl_6:10% Er^{3+}, 0.1% Os^{4+} and Cs_2NaYCl_6:10% Er^{3+} excited at 10 959 and 10 492 cm^{-1}, respectively. The Er^{3+} transitions are labeled with the emitting levels $^4F_{9/2}$, $^4S_{3/2}$, and $^2H_{9/2}$, whereas the initial and final levels are given for the Os^{4+} transitions.

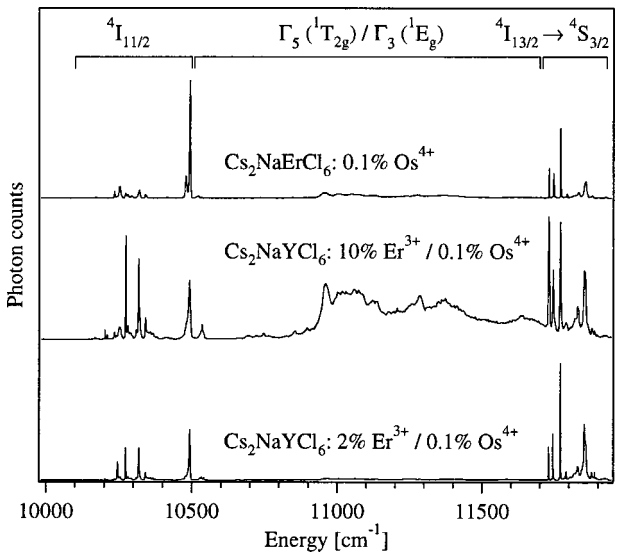

FIG. 4. 15-K upconversion-excitation spectra of Cs_2NaYCl_6:x% Er^{3+}, 0.1% Os^{4+} ($x=2$, 10, and 100) detecting the $^4S_{3/2}\rightarrow{}^4I_{15/2}$ transition at 18 154 cm^{-1}. Various excitation regions are assigned.

centered around 5000, 11 000, and 17 000 cm^{-1} in the Cs_2NaYCl_6:0.1% Os^{4+} spectrum are assigned to $\Gamma_5/\Gamma_3(^3T_{1g})$, $\Gamma_5(^1T_{2g})/\Gamma_3(^1E_g)$, and $\Gamma_1(^1A_{1g})$, respectively. The strong increase in absorption above 23 000 cm^{-1} is to the first $Cl^-\rightarrow Os^{4+}$ charge-transfer band.

Figure 3 compares the upconversion-luminescence spectra of Cs_2NaYCl_6:10% Er^{3+} and Cs_2NaYCl_6:10% Er^{3+},0.1% Os^{4+} excited at 10 492 and 10 959 cm^{-1}, respectively. The multiplets in the Cs_2NaYCl_6:10% Er^{3+} spectrum centered around 15 000, 18 000, and 24 000 cm^{-1} are assigned to the transitions from $^4F_{9/2}$, $^4S_{3/2}$, and $^2H_{9/2}$, respectively, to the ground state $^4I_{15/2}$. The $^4F_{9/2}$ and $^4S_{3/2}$ multiplets also appear in the Cs_2NaYCl_6:10% Er^{3+},0.1% Os^{4+} crystal, whereas the $^2H_{9/2}$ multiplet is only barely visible. The $^4S_{3/2}$ luminescence intensity depends quadratically on the power of the 10 959-cm^{-1} excitation. The additional bands centered around 17 000 and 14 000 cm^{-1} are assigned to the Os^{4+} transitions $\Gamma_1(^1A_{1g})\rightarrow\Gamma_1(^3T_{1g})$ and $\Gamma_1(^1A_{1g})\rightarrow\Gamma_4(^3T_{1g})$, respectively.

Figure 4 shows the 15-K upconversion excitation spectra of Cs_2NaYCl_6:2% Er^{3+}, 0.1% Os^{4+}, Cs_2NaYCl_6:10% Er^{3+}, 0.1% Os^{4+}, and $Cs_2NaErCl_6$:0.1% Os^{4+}, detecting the $^4S_{3/2}$ luminescence at 18 154 cm^{-1}. The spectra are composed of three characteristic regions. Below 10 500 cm^{-1} and above 11 700 cm^{-1}, two multiplets of sharp lines are observed. The spectrum below 10 500 cm^{-1} coincides with the Er^{3+} absorption in Fig. 2(a), and is consequently assigned to $^4I_{15/2}\rightarrow{}^4I_{11/2}$ excitations. No equivalent of the multiplet observed above 11 700 cm^{-1} is found in the absorption spectra of Figs. 2(a) and 2(b). It is assigned to the $^4I_{13/2}\rightarrow{}^4S_{3/2}$ ESA on Er^{3+}. The broad and slightly structured band observed between 10 700 and 11 900 cm^{-1} in the excitation spectrum of Cs_2NaYCl_6:10% Er^{3+},0.1% Os^{4+} coincides with the absorption band of Cs_2NaYCl_6:0.1% Os^{4+} depicted in Fig. 2(b) and is consequently assigned to the $\Gamma_1(^3T_{1g})\rightarrow\Gamma_5(^1T_{2g})/\Gamma_3(^1E_g)$ excitation of Os^{4+}. This broad band is only barely visible in the Cs_2NaYCl_6:2% Er^{3+}, 0.1% Os^{4+} and $Cs_2NaErCl_6$:0.1% Os^{4+} spectra. Only the sharp lines below 10 500 cm^{-1} can be observed in the analogous excitation spectrum of Cs_2NaYCl_6:10% Er^{3+}.

Figure 5 shows the 15-K $\Gamma_1(^1A_{1g})\rightarrow\Gamma_1(^3T_{1g})$ luminescence transition in Cs_2NaYCl_6:0.1% Os^{4+} excited at 10 959 and 11 285 cm^{-1}, respectively. The fine structures observed for the two excitations are different. In Fig. 6 the 15-K excitation spectra of the $\Gamma_1(^1A_{1g})\rightarrow\Gamma_1(^3T_{1g})$ luminescence in Cs_2NaYCl_6:0.1% Os^{4+} detected at 16 870 and 16 896 cm^{-1}, respectively, are compared with the 15-K absorption spectrum of the same compound. The excitation spectrum of the

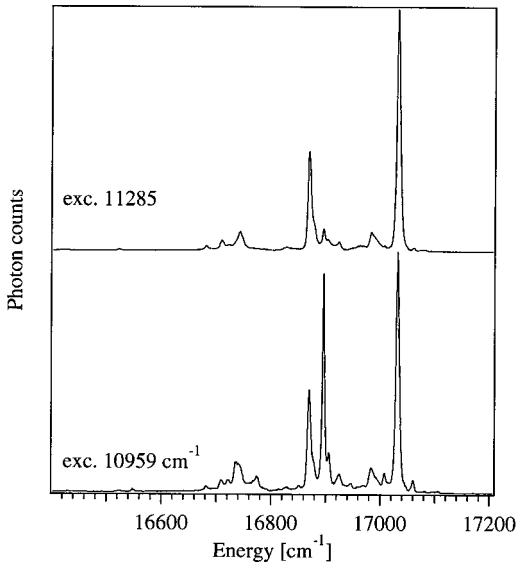

FIG. 5. 15-K upconversion-luminescence spectra of Cs_2NaYCl_6:0.1% Os^{4+} excited at 11 285 and 10 959 cm^{-1}.

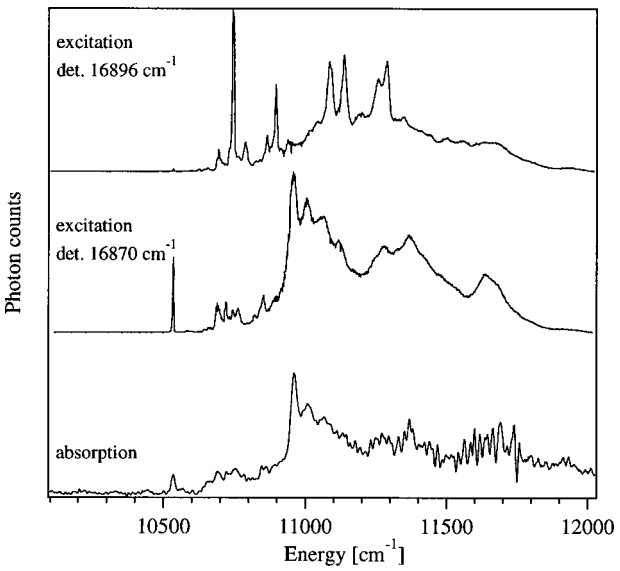

FIG. 6. 15-K upconversion-excitation spectra of Cs_2NaYCl_6:0.1% Os^{4+}, detecting the luminescence at 16 870 and 16 896 cm^{-1} in comparison to the absorption of the same compound in this spectral region.

16 870-cm^{-1} luminescence coincides in line positions and relative intensities with the absorption spectrum, whereas the 16 896-cm^{-1} excitation spectrum shows a different fine structure.

Figure 7 shows the 15-K infrared luminescence spectrum of Cs_2NaYCl_6:10% Er^{3+}, 0.1% Os^{4+} excited at 10 959 cm^{-1}. The spectrum is dominated by the lines around 6500 cm^{-1} assigned to the Er^{3+} transition $^4I_{13/2} \rightarrow {}^4I_{15/2}$. The spectral region between 6600 and 10 500 cm^{-1}, shown in the inset to Fig. 7 is enlarged by a factor of 125. It consists of the Os^{4+} $\Gamma_5(^1T_{2g})/\Gamma_3(^1E_g) \rightarrow \Gamma_1(^3T_{1g})$ and $\Gamma_5(^1T_{2g})/\Gamma_3(^1E_g) \rightarrow \Gamma_4(^3T_{1g})$ transitions, and the Er^{3+} $^4I_{11/2}/2 \rightarrow {}^4I_{15/2}$ transition, centered around 10 300, 7500, and 10 000 cm^{-1}, respectively. The ratios of the

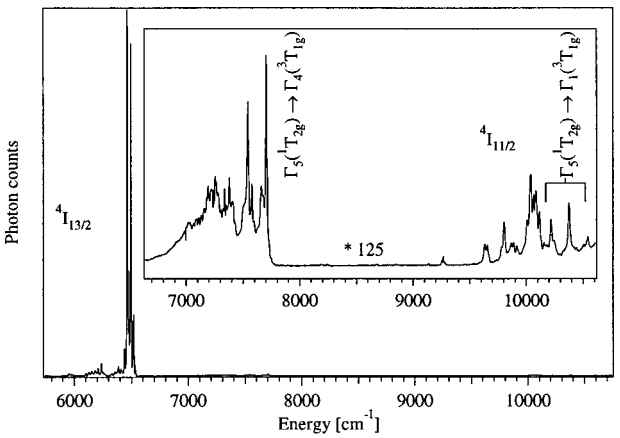

FIG. 7. 15-K NIR luminescence of Cs_2NaYCl_6:10% Er^{3+}, 0.1% Os^{4+} excited at 10 959 cm^{-1}. The inset shows a 125 times enlarged view of the 6600–10 500-cm^{-1} region. The Er^{3+} transitions are labeled with the emitting levels $^4I_{11/2}$ and $^4I_{13/2}$, whereas the initial and final levels are given for the Os^{4+} transitions.

TABLE I. Ratios of the 15-K $^4I_{13/2} \rightarrow {}^4I_{15/2}$ to $^4I_{11/2} \rightarrow {}^4I_{15/2}$ photon fluxes detected at 6462 and 9803 cm^{-1}, respectively, in Cs_2NaYCl_6 crystals doped with Er^{3+} and Os^{4+}, as indicated in the left column. The ratios were determined for the excitations into $^4I_{11/2}$ and $\Gamma_5(^1T_{2g})/\Gamma_3(^1E_g)$ at 10 492 and 10 959 cm^{-1}, respectively.

	exc. 10 492 cm^{-1}	exc. 10 959 cm^{-1}
2% Er^{3+}	28	
2% Er^{3+}, 0.1% Os^{4+}	100	14 200
10% Er^{3+}, 0.1% Os^{4+}	110	1100
100% Er^{3+}, 0.1% Os^{4+}	1670	2860

$^4I_{13/2} \rightarrow {}^4I_{15/2}$ to $^4I_{11/2} \rightarrow {}^4I_{15/2}$ photon fluxes detected at 6462 and 9803 cm^{-1}, respectively, are collected in Table I for the 10 492- and 10 959-cm^{-1} excitation energies. These ratios are strongly dependent on the Er^{3+} concentration, and considerably larger in the crystals codoped with Er^{3+} and Os^{4+} than in the samples singly doped with Er^{3+}.

The 15-K excitation spectra of the $^4I_{13/2} \rightarrow {}^4I_{15/2}$ and $^4I_{11/2} \rightarrow {}^4I_{15/2}$ luminescence bands of Cs_2NaYCl_6:10% Er^{3+},0.1% Os^{4+} detected at 6462 and 9803 cm^{-1}, respectively, are shown in Fig. 8. The series of sharp lines observed below 10 500 cm^{-1} is assigned to $^4I_{15/2} \rightarrow {}^4I_{11/2}$. The broad band above 10 500 cm^{-1} is assigned to $\Gamma_1(^3T_{1g}) \rightarrow \Gamma_5(^1T_{2g})/\Gamma_3(^1E_g)$. The relative intensity of the broad band is higher by one order of magnitude in the excitation spectrum monitoring the $^4I_{13/2} \rightarrow {}^4I_{15/2}$ transition.

The 15-K $^4S_{3/2}$, $^4I_{11/2}$, $\Gamma_1(^1A_{1g})$, and $\Gamma_5(^1T_{2g})/\Gamma_3(^1E_g)$ lifetimes of Cs_2NaYCl_6, doped with various concentrations of Er^{3+} and Os^{4+}, were determined from single exponential luminescence decays. They are collected in

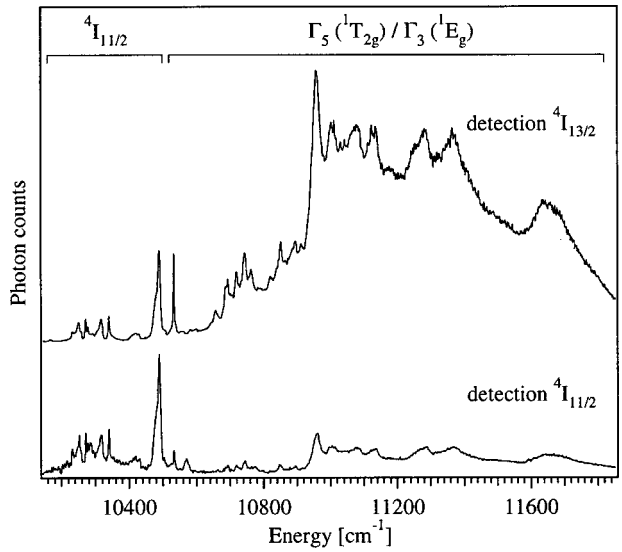

FIG. 8. 15-K excitation spectra of Cs_2NaYCl_6:10% Er^{3+}, 0.1% Os^{4+} monitoring the $^4I_{11/2} \rightarrow {}^4I_{15/2}$ and $^4I_{13/2} \rightarrow {}^4I_{15/2}$ transitions at 9803 and 6462 cm^{-1}, respectively. The Os^{4+} $\Gamma_5(^1T_{2g})/\Gamma_3(^1E_g)$ and Er^{3+} $^4I_{11/2}$ excitation regions are assigned.

TABLE II. 15-K luminescence decay times obtained from single-exponential fits to the experimentally observed transients. The left column gives the doping concentrations of Er^{3+} and Os^{4+} in the Cs_2NaYCl_6 host.

	$\Gamma_1(^1A_{1g})$	$\Gamma_5(^1T_{2g})/\Gamma_3(^1E_g)$	$^4S_{3/2}$	$^4I_{11/2}$
0.1% Os^{4+}	16.5 μs	199 μs		
2% Er^{3+}			11.2 ms	83.6 ms
10% Er^{3+}			11.0 ms	45 ms
0.1% Os^{4+} 2% Er^{3+}	2.8 μs	97 μs	7.5 ms	56 ms
0.1% Os^{4+} 10% Er^{3+}	3.6 μs	120 μs	7.2 ms	12 ms
0.1% Os^{4+} 100% Er^{3+}	0.2 μs	<1 μs	119 μs	1.2 ms

Table II. The lifetimes of the codoped samples are shorter than those of the singly doped crystals.

IV. DISCUSSION

A. Os^{4+} in Cs_2NaYCl_6

The optical spectroscopy of Os^{4+} doped into cubic halide lattices is well known.[9–11,16–21] Common hosts are Cs_2GeF_6, Cs_2ZrCl_6, and Cs_2ZrBr_6, in which Os^{4+} replaces the octahedrally coordinated tetravalent ions. Os^{4+} has a $5d^4$ electron configuration, giving rise to a $^3T_{1g}$ ground state in octahedral symmetry; see Fig. 1. This ground state is split into Γ_1, Γ_4, Γ_5, and Γ_3, with a total spread of 5000 cm^{-1} in Cs_2ZrCl_6: Os^{4+}. The ligand field experienced by the $5d$ electrons is so high that the interconfigurationally excited states arising from the strong-field $(t_{2g})^3(e_g)^1$ electron configuration are not found within the visible spectral range. The lowest energy excitations in Cs_2ZrCl_6: Os^{4+} are the spin flips within the $(t_{2g})^4$ electron configuration around 11 000 and 17 000 cm^{-1}, assigned to $\Gamma_5(^1T_{2g})/\Gamma_3(^1E_g)$ and $\Gamma_1(^1A_{1g})$, respectively.[21] Above 23 000 cm^{-1} $Cl^-\rightarrow Os^{4+}$ charge-transfer (CT) bands are observed.[18]

Cs_2NaYCl_6 (Ref. 22) and Cs_2OsCl_6 (Ref. 23) both crystallize in the cubic $Fm3m$ space group with unit-cell constants $a=10.73$ and 10.21 Å, respectively. The two structures are thus closely related, and the Y^{3+} and Os^{4+} sites in the two structures are both octahedrally coordinated by Cl^-. Removing Na^+ ions located on the middle of the edges of the cubic unit cell transforms the Cs_2NaYCl_6 elpasolite structure into the Cs_2OsCl_6 antifluorite structure. Due to the charge difference between the Os^{4+} dopant ion and the Y^{3+} lattice site, only a limited concentration of Os^{4+} can be doped into Cs_2NaYCl_6. Our crystals only contain 0.1% Os^{4+}, even though a nominal concentration of 2% was used in the synthesis. The fact that the absorption spectrum in Fig. 2(b) is similar to the Cs_2ZrCl_6: Os^{4+} spectrum[21] proves that most of the Os is incorporated as Os^{4+}.

The Os^{4+} ions are assumed to substitute for Y^{3+} on O_h sites in Cs_2NaYCl_6. To compensate for the charge difference, most probably one of the six nearest Na^+ positions is vacant. This vacancy in the second coordination sphere removes the inversion symmetry around Os^{4+}. This is why, in contrast to the analogous transitions in Cs_2ZrCl_6: Os^{4+},[21] an electronic-origin intensity is observed in the absorption and luminescence transitions. The fact that a considerable part of the intensity still lies in vibronic origins, which acquire an electric dipole intensity by coupling of ungerade modes to the electronic transitions, indicates only a slight deviation from the octahedral symmetry.

Some very weak and relatively broad bands are observed around 14 500, 16 000, and 21 000 cm^{-1} in Fig. 2(b). These bands do not belong to the octahedral Os^{4+} chromophore. Whereas the broad 14 500-cm^{-1} band might be due to a baseline uncertainty, the other two bands are certainly real. They cannot unambiguously be assigned, and we suggest two tentative explanations based on the hypothetical occurrence of an Os^{3+} species or Os^{4+} dimers in our sample: Cs_2NaYCl_6 might conceivably stabilize an $OsCl_6^{3-}$ species. The absorption of $OsCl_6^{3-}$ in chloride melts and aqueous HCl solutions has been published.[24,25] These publications were mainly concerned with the intense CT absorption bands occurring above 25 000 cm^{-1}, and can thus not help assigning the weak features observed around 16 000 and 21 000 cm^{-1} in Fig. 2(b). However, these weak bands could be due to d-d bands of $OsCl_6^{3-}$ occurring below 25 000 cm^{-1}. Although we cannot exclude this possibility, we prefer to assign the 16 000- and 21 000-cm^{-1} bands observed in the Cs_2NaYCl_6: 0.1% Os^{4+} absorption spectrum to pair excitations.

Bands in the 15 000- and 22 000-cm^{-1} regions were observed in the absorption spectra of the $Os_2Cl_{10}^{2-}$ chromophore, consisting of two edge-sharing $OsCl_6^{2-}$ units.[26] They were assigned as dimer excitations. Also, in concentrated $OsCl_6^{2-}$ compounds such as K_2OsCl_6 or Cs_2OsCl_6, bands were observed below $\Gamma_1(^1A_{1g})$, and assigned to pair transitions.[27,28] Assigning the 16 000-cm^{-1} band in the absorption spectrum of Fig. 2 to a pair transition implies that some of the Os^{4+} ions aggregate as clusters in Cs_2NaYCl_6. These clusters might be favored in the Cs_2NaYCl_6 host by the need for charge compensation, leading to Os^{4+} clusters with a Cs_2OsCl_6 structure.

Below 150 K, Cs_2ZrCl_6:Os^{4+} shows luminescence originating from $\Gamma_5(^1T_{2g})/\Gamma_3(^1E_g)$ and $\Gamma_1(^1A_{1g})$. In Cs_2ZrCl_6: 0.1% Os^{4+}, 15-K lifetimes of 483 and 29 μs, respectively, were found.[11] We recently reported that Cs_2ZrCl_6:Os^{4+} shows $\Gamma_1(^1A_{1g})$ upconversion luminescence after $\Gamma_5(^1T_{2g})/\Gamma_3(^1E_g)$ excitation.[11] Figure 5 shows that Cs_2NaYCl_6:0.1% Os^{4+} also exhibits $\Gamma_1(^1A_{1g})\rightarrow\Gamma_1(^3T_{1g})$ upconversion luminescence. The fine structures of the two spectra excited at 11 285 and 10 959 cm^{-1}, respectively, are slightly different. We ascribe this difference to the presence of at least two Os^{4+} sites with slightly different environments. The two upconversion-excitation spectra in Fig. 6, monitoring the $\Gamma_1(^1A_{1g})\rightarrow\Gamma_1(^3T_{1g})$ transition at 16 896 and 16 870 cm^{-1}, respectively, also show different fine structures. The excitation spectrum measured at the 16 870-cm^{-1} detection energy is very similar to the absorption spectrum of Cs_2NaYCl_6: 0.1% Os^{4+}, and is thus attributed to the main site. This spectrum peaks at 10 959 cm^{-1}. By 10 959-cm^{-1} excitation this main site can thus selectively be excited.

The 15-K luminescence-decay times of the main Os^{4+} site in Cs_2NaYCl_6 are $\tau = 199$ and 16 μs for $\Gamma_5(^1T_{2g})/\Gamma_3(^1E_g)$ and $\Gamma_1(^1A_{1g})$, respectively; see Table II. They are thus shorter than the corresponding 483 and 29 μs in Cs_2ZrCl_6: 0.1% Os^{4+} at the same temperature.

B. Er^{3+} in Cs_2NaYCl_6

In contrast to d-d transitions of transition-metal ions, the energies of f-f excited states in lanthanides are almost independent of the chemical environment. Their energetic positions are mainly determined by spin-orbit coupling and Coulomb repulsion. The splitting of the individual multiplets induced by the crystal field is in the range of a few hundred wave numbers. A detailed analysis of the $Cs_2NaErCl_6$ energy levels is contained in Ref. 29.

All the f-f absorptions in Fig. 2 are very weak. ϵ values lie in the range between 0.1 and 4 $l\,mol^{-1}\,cm^{-1}$, and are thus significantly weaker than the intraconfiguration transitions of Cs_2NaYCl_6:Os^{4+}, with ϵ values between 5 and 180 $l\,mol^{-1}\,cm^{-1}$. All the electronic f-f transitions are parity forbidden because of the exactly octahedral coordination of Er^{3+}. The electric-dipole (ED) intensity is therefore only observed in vibronic sidebands. The $^4I_{15/2} \rightarrow {}^4I_{13/2}$ transition around 6000 cm^{-1} is magnetic dipole (MD) allowed, and thus more intense than the other f-f transitions in Fig. 2(a), which are all MD forbidden. Its intensity is mainly contained in the MD electronic origins, which are followed by the weak ED vibronic origins to higher energy.

Er^{3+} is a very prominent upconversion ion. After excitation into the intermediate states $^4I_{13/2}$, $^4I_{11/2}$, and $^4I_{9/2}$ around 6000, 10 000, and 12 000 cm^{-1}, respectively, efficient red, green, and blue upconversion luminescence is observed in many Er^{3+}-doped crystals and glasses. This is due to the favorable energy-level scheme of Er^{3+} with series of almost equally spaced multiplets; see Fig. 1. $^2H_{9/2}$ and $^4F_{7/2}$ almost exactly lie at twice the energy of $^4I_{9/2}$ and $^4I_{11/2}$, respectively, and can thus be reached resonantly by two-step processes involving $^4I_{9/2}$ and $^4I_{11/2}$. Exciting $^4I_{13/2}$ at roughly half the energy of $^4I_{9/2}$ leads to upconversion luminescence involving the absorption of up to four excitation quanta.[30]

Upconversion has been observed and reported in Er^{3+}-doped chloride elpasolites[31,32] $^4I_{11/2}$, $^4I_{9/2}$, and $^4F_{9/2}$ served as excitation levels. The lower part of Fig. 3 shows the 15-K upconversion-luminescence spectrum of Cs_2NaYCl_6:10% Er^{3+} excited into $^4I_{11/2}$. Bands in the blue, green, and red spectral regions are observed, leading to an upconversion luminescence that appears greenish white to the eye. The bands around 24 000, 18 000, and 15 000 cm^{-1} are assigned to $^2H_{9/2}$, $^4S_{3/2}$, and $^4F_{9/2} \rightarrow {}^4I_{15/2}$, respectively. Note that more than two 10 492-cm^{-1} quanta are needed to populate the $^2H_{9/2}$ multiplet at 24 000 cm^{-1}.

The 15-K $^4S_{3/2}$ and $^4I_{11/2}$ lifetimes of Cs_2NaYCl_6:10% Er^{3+} are 11.0 and 45 ms, respectively. We find a considerably longer 15-K $^4I_{11/2}$ lifetime of 83.6 ms in Cs_2NaYCl_6: 2% Er^{3+} than the $\tau = 45$ ms determined for $^4I_{11/2}$ in Cs_2NaYCl_6:10% Er^{3+}, whereas the $^4S_{3/2}$ lifetime of $\tau = 11.2$ ms is essentially identical to the $\tau = 11.0$ ms found in Cs_2NaYCl_6:10% Er^{3+}; see Table II. We attribute the reduced $^4I_{11/2}$ lifetime in the more concentrated crystal to an energy-transfer upconversion process $^4I_{11/2} + {}^4I_{11/2} \rightarrow {}^4I_{15/2} + {}^4F_{7/2}$, that acts as a relaxation pathway for the $^4I_{11/2}$ population.

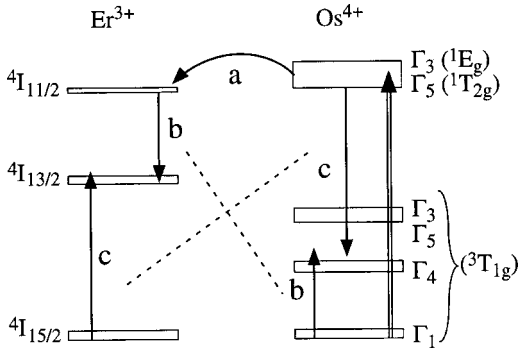

FIG. 9. Nonradiative energy-transfer processes between Os^{4+} and Er^{3+} after excitation into $\Gamma_5(^1T_{2g})/\Gamma_3(^1E_g)$. The bent arrow shows the transfer of the whole Os^{4+} excitation energy to Er^{3+}. Cross-relaxations are indicated with pairs of arrows connected with dashed lines. The labeling of the processes is identical to the one used in Sec. IV C 1.

C. Cooperative processes between Os^{4+} and Er^{3+}

1. Energy transfer from $\Gamma_5(^1T_{2g})/\Gamma_3(^1E_g)$ on Os^{4+} to $^4I_{11/2}$ and $^4I_{13/2}$ on Er^{3+}

In this section we focus on the energy-transfer steps occurring between Os^{4+} and Er^{3+} after excitation into $\Gamma_5(^1T_{2g})/\Gamma_3(^1E_g)$ around 11 000 cm^{-1}. These initial steps are the basis for subsequent upconversion processes, that will be discussed in Sec. IV C 2. Figure 9 shows a schematic energy-level diagram of the Os^{4+} and Er^{3+} states below 12 000 cm^{-1}. Based on energy arguments, three nonradiative energy-transfer processes labeled *a*, *b*, and *c* in Fig. 9 can occur. Process *a* represents the transfer of the $\Gamma_5(^1T_{2g})/\Gamma_3(^1E_g)$ energy to $^4I_{11/2}$. This process is characterized by only a small energy difference $\Delta E = 325\ cm^{-1}$ between the electronic origins of $\Gamma_5(^1T_{2g})/\Gamma_3(^1E_g)$ and the highest $^4I_{11/2}$ crystal-field level, and is consequently expected to be efficient.

Process *a* can be followed by process *b*, a cross-relaxation process by which $^4I_{11/2}$ relaxes to $^4I_{13/2}$ exciting a neighboring Os^{4+} ion from the ground state to $\Gamma_4(^3T_{1g})$. Process *b* is expected to be less efficient than process *a*, due to the bigger energy difference $\Delta E = 638\ cm^{-1}$ between the $^4I_{11/2} \rightarrow {}^4I_{13/2}$ and $\Gamma_1(^3T_{1g}) \rightarrow \Gamma_4(^3T_{1g})$ transitions. Process *c*, finally, describes the cross-relaxation, by which part of the Os^{4+} $\Gamma_5(^1T_{2g})/\Gamma_3(^1E_g)$ energy is transferred to Er^{3+}, exciting the Er^{3+} ion to $^4I_{13/2}$ and leaving the Os^{4+} ion in $\Gamma_4(^3T_{1g})$. This energy-transfer process is characterized by $\Delta E = 1020\ cm^{-1}$ between the $\Gamma_5(^1T_{2g})/\Gamma_3(^1E_g) \rightarrow \Gamma_4(^3T_{1g})$ and $^4I_{15/2} \rightarrow {}^4I_{13/2}$ transitions, and is thus expected to be the least efficient of the three processes.

Figure 8, showing the 15-K excitation spectrum of the $^4I_{11/2}$ luminescence of Cs_2NaYCl_6:10% Er^{3+}, 0.1% Os^{4+} demonstrates that process *a* occurs in Cs_2NaYCl_6 codoped

with Er^{3+} and Os^{4+}. In addition to the sharp lines below 10 500 cm^{-1} characteristic of the direct $^4I_{11/2}$ excitation, we find the structured band above 10 500 cm^{-1} typical for the Os^{4+} $\Gamma_5(^1T_{2g})/\Gamma_3(^1E_g)$ excitation. This is direct evidence of process *a*, transferring part of the initial Os^{4+} excitation to $^4I_{11/2}$ of Er^{3+}.

The efficiency of process *b* can be estimated by comparing the ratios of the $^4I_{13/2}\rightarrow{}^4I_{15/2}$ to $^4I_{11/2}\rightarrow{}^4I_{15/2}$ photon fluxes in the codoped Cs_2NaYCl_6:Er^{3+}, Os^{4+} samples, with the corresponding ratios observed in the singly doped Cs_2NaYCl_6:Er^{3+} crystals. The ratios of these photon fluxes, detected at 6462 and 9803 cm^{-1}, respectively, are collected in Table I for $^4I_{11/2}$ excitation. Already in the singly doped Cs_2NaYCl_6:2% Er^{3+} crystal, the $^4I_{13/2}\rightarrow{}^4I_{15/2}$ luminescence band dominates. Its photon flux is larger by a factor of 28 than the $^4I_{11/2}\rightarrow{}^4I_{15/2}$ photon flux. The energy gap between $^4I_{11/2}$ and $^4I_{13/2}$ is too large to attribute this observation to an efficient $^4I_{11/2}\rightarrow{}^4I_{13/2}$ multiphonon relaxation, and also cross-relaxations cannot induce a relaxation from $^4I_{11/2}$ to $^4I_{13/2}$ in the singly doped Cs_2NaYCl_6:2% Er^{3+} sample. We thus conclude that $^4I_{13/2}$ is fed by the radiative $^4I_{11/2}\rightarrow{}^4I_{13/2}$ transition. This implies a large radiative $^4I_{11/2}\rightarrow{}^4I_{13/2}$ to $^4I_{11/2}\rightarrow{}^4I_{15/2}$ branching ratio.

The ratio of the $^4I_{13/2}\rightarrow{}^4I_{15/2}$ to $^4I_{11/2}\rightarrow{}^4I_{15/2}$ photon fluxes increases from 28 to 100 between the singly doped Cs_2NaYCl_6:2% Er^{3+} and the codoped Cs_2NaYCl_6:2% Er^{3+}, 0.1% Os^{4+}, and this is ascribed to process *b*. In Cs_2NaYCl_6:10% Er^{3+}, 0.1% Os^{4+} and $Cs_2NaErCl_6$:0.1% Os^{4+}, the corresponding ratios are 110 and 1670; see Table I. This concentration dependence is due to an energy migration that significantly increases the probability to bring an Er^{3+} $^4I_{11/2}$ excitation into the neighborhood of an Os^{4+} ion. The higher the Er^{3+} concentration, the more mobile the $^4I_{11/2}$ excitation becomes, thus increasing the efficiency of process *b*. This increase is accompanied by a decrease of the $^4I_{11/2}$ lifetime from 83.6 ms in Cs_2NaYCl_6: 2% Er^{3+} to 56, 12, and 1.2 ms in the codoped samples Cs_2NaYCl_6:*x*% Er^{3+},0.1% Os^{4+}, with $x=2$, 10, and 100, respectively.

According to Fig. 9, process *c* is in competition with the sequence $a+b$ for populating $^4I_{13/2}$ after initial $\Gamma_5(^1T_{2g})/\Gamma_3(^1E_g)$ excitation. Comparing the excitation spectra of the $^4I_{11/2}\rightarrow{}^4I_{15/2}$ and $^4I_{13/2}\rightarrow{}^4I_{15/2}$ luminescence transitions of Cs_2NaYCl_6:10% Er^{3+}, 0.1% Os^{4+} in Fig. 8 reveals that $^4I_{13/2}$ is predominantly fed by $\Gamma_5(^1T_{2g})/\Gamma_3(^1E_g)$ excitation above 10 500 cm^{-1}, in contrast to $^4I_{11/2}$. This increased Os^{4+} contribution in the feeding of $^4I_{13/2}$ can thus plausibly be attributed to process *c* bypassing the $^4I_{11/2}$ state by the direct energy-transfer step $\Gamma_5(^1T_{2g})/\Gamma_3(^1E_g)\rightarrow{}^4I_{13/2}$.

Unfortunately, this plausible explanation is not as unambiguous as it looks at first sight. The difference in the NIR excitation spectra of Fig. 8 can also be explained within the $a+b$ sequence of processes. This alternative interpretation is based on the fact that different subsets of Er^{3+} ions in the crystal are excited by process *a* and by direct $^4I_{11/2}$ excitation: Direct $^4I_{11/2}$ excitation is unselective with respect to the Er^{3+} environment, whereas energy transfer from $\Gamma_5(^1T_{2g})$ by process *a* primarily excites Er^{3+} ions neighboring the initially excited Os^{4+} ions. For this latter subset of Er^{3+} ions, process *b* is more likely to occur than for the majority of directly excited Er^{3+} ions, leading to the large relative intensity of the Os^{4+} bands above 10 500 cm^{-1} in the excitation spectrum monitoring the $^4I_{13/2}$ luminescence.

The analysis of process *b* has revealed the importance of energy migration among the Er^{3+} ions. This migration is also a key factor in determining the efficiency of the $a+b$ sequence of processes after excitation into $\Gamma_5(^1T_{2g})/\Gamma_3(^1E_g)$. A sequence of $a+b$ processes taking place in a given Os^{4+}-Er^{3+} pair is most likely in crystals with low Er^{3+} concentration. At higher Er^{3+} concentrations, energy migration away from this active center becomes competitive. We thus expect to find the highest ratio of the $^4I_{13/2}\rightarrow{}^4I_{15/2}$ to $^4I_{11/2}\rightarrow{}^4I_{15/2}$ photon fluxes in the codoped sample with the lowest Er^{3+} concentration upon Os^{4+} $\Gamma_5(^1T_{2g})/\Gamma_3(^1E_g)$ excitation. This is exactly what we observe; see Table I. The largest ratio of 14 200 is found for the Cs_2NaYCl_6:2% Er^{3+},0.1% Os^{4+} crystal. It then decreases to 1100 in Cs_2NaYCl_6:10% Er^{3+},0.1% Os^{4+}, and increases again to 2860 in $Cs_2NaErCl_6$:0.1% Os^{4+}. All these values are larger by at least one order of magnitude than the corresponding ratios observed after direct $^4I_{11/2}$ excitation, indicating an enhanced probability of process *b* for those Er^{3+} ions neighboring Os^{4+}. The concentration dependence could not be explained by process *c*, and we conclude that the $a+b$ sequence of processes is the predominant pathway to populate $^4I_{13/2}$ after $\Gamma_5(^1T_{2g})/\Gamma_3(^1E_g)$ excitation.

Process *a* is thus identified as the initial energy-transfer step after $\Gamma_5(^1T_{2g})/\Gamma_3(^1E_g)$ excitation in all the Cs_2NaYCl_6 crystals codoped with Er^{3+} and Os^{4+}. It causes a decrease of the $\Gamma_5(^1T_{2g})/\Gamma_3(^1E_g)$ lifetime from 199 μs in Cs_2NaYCl_6:0.1% Os^{4+} to 120 μs in Cs_2NaYCl_6:10% Er^{3+}, 0.1% Os^{4+}; see Table II. In $Cs_2NaErCl_6$:0.1% Os^{4+} hardly any $\Gamma_5(^1T_{2g})/\Gamma_3(^1E_g)\rightarrow\Gamma_1(^3T_{1g})$ luminescence is observed, and the corresponding lifetime is shorter than 1 μs. In the $Cs_2NaErCl_6$ host every Os^{4+} ion is surrounded by several Er^{3+} ions in the nearest neighborhood, making process *a* the most efficient decay channel for $\Gamma_5(^1T_{2g})$. At low Er^{3+} concentrations, the $\Gamma_5(^1T_{2g})/\Gamma_3(^1E_g)$ population is predominantly transferred to $^4I_{13/2}$ by the $a+b$ sequence, whereas at higher Er^{3+} concentration part of the $^4I_{11/2}$ excitation induced by process *a* persists. The branching between $\Gamma_5(^1T_{2g})/\Gamma_3(^1E_g)\rightarrow{}^4I_{11/2}$ and $\Gamma_5(^1T_{2g})/\Gamma_3(^1E_g)\rightarrow{}^4I_{13/2}$ can thus be tuned by the Er^{3+} concentration.

2. Green Er^{3+} upconversion luminescence after $\Gamma_5(^1T_{2g})/\Gamma_3(^1E_g)$ excitation on Os^{4+}

Processes I, II, and III, schematically depicted in Fig. 10, lead to green Er^{3+} upconversion luminescence after $\Gamma_5(^1T_{2g})/\Gamma_3(^1E_g)$ excitation on Os^{4+}. Process I represents the upconversion process usually observed in compounds singly doped with Er^{3+} upon $^4I_{11/2}$ excitation, by which $^4F_{7/2}$ is initially excited, followed by fast multiphonon relaxation to $^4S_{3/2}$. As the $^4I_{15/2}\rightarrow{}^4I_{11/2}$ GSA is almost resonant to the $^4I_{11/2}\rightarrow{}^4F_{7/2}$ ESA, both GSA/ETU and GSA/ESA mechanisms can induce upconversion in compounds singly

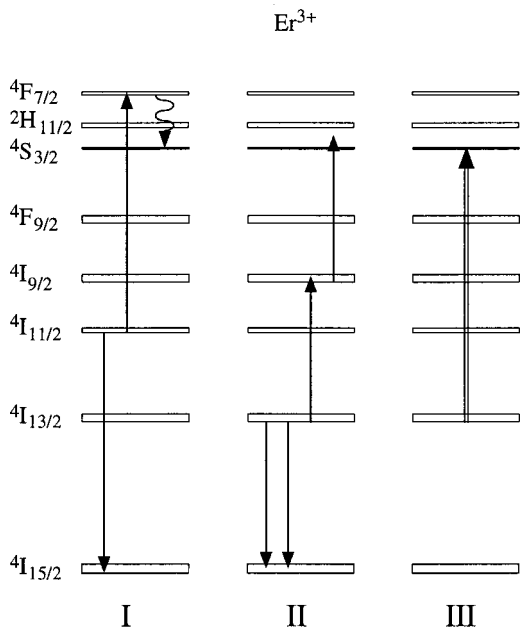

FIG. 10. Upconversion processes leading to $^4S_{3/2}$ luminescence starting from $^4I_{11/2}$ (I) and $^4I_{13/2}$ (II and III). The solid, curly, and double arrows represent energy-transfer upconversion, multiphonon relaxation, and excited-state absorption, respectively.

doped with Er^{3+}. As the laser tuned to the $\Gamma_5(^1T_{2g})/\Gamma_3(^1E_g)$ states of Os^{4+} is too high in energy for a resonant $^4I_{11/2}\rightarrow{}^4F_{7/2}$ ESA step, we assume the upconversion step in scheme I to occur by energy transfer. Scheme II indicates an energy-transfer upconversion mechanism starting from $^4I_{13/2}$, reaching $^4I_{9/2}$ in a first step followed by a second energy-transfer step to populate $^4S_{3/2}$. In contrast to fluorides and oxides, $^4I_{9/2}$ is metastable in chlorides, and this upconversion scheme has been shown to work efficiently.[30] Processes I and II consume two and three excitation photons, respectively, to create one $^4S_{3/2}$ excitation and should consequently be characterized by quadratic and cubic dependencies, respectively, of the $^4S_{3/2}$ upconversion-luminescence intensity on the excitation power.

Process III is the ESA from $^4I_{13/2}$ to $^4S_{3/2}$. This process cannot be induced by single-color excitation in compounds singly doped with Er^{3+}, as Er^{3+} is transparent at the $^4I_{13/2}\rightarrow{}^4S_{3/2}$ ESA energy above 11 700 cm^{-1}. In contrast, Os^{4+} absorbs at this wavelength. The sequence of absorption on Os^{4+}, energy transfer to $^4I_{13/2}$, and ESA $^4I_{13/2}\rightarrow{}^4S_{3/2}$ might thus occur, and represent an upconversion mechanism of Os^{4+} and Er^{3+} in the codoped Cs_2NaYCl_6 crystals.

Figure 3 demonstrates that Os^{4+} sensitization of Er^{3+} upconversion occurs in Cs_2NaYCl_6 codoped with Os^{4+} and Er^{3+}. It shows the upconversion luminescence of Cs_2NaYCl_6:10% Er^{3+},0.1% Os^{4+} upon $\Gamma_5(^1T_{2g})/\Gamma_3(^1E_g)$ excitation of Os^{4+}. In addition to the Os^{4+} $\Gamma_1(^1A_{1g})\rightarrow\Gamma_1(^3T_{1g})$ and $\Gamma_1(^1A_{1g})\rightarrow\Gamma_4(^3T_{1g})$ upconversion-luminescence bands, we observe the $^4S_{3/2}\rightarrow{}^4I_{15/2}$ and $^4F_{9/2}\rightarrow{}^4I_{15/2}$ Er^{3+} upconversion-luminescence transitions. The excitation spectrum of the $^4S_{3/2}$ upconversion luminescence in Cs_2NaYCl_6:10% Er^{3+},0.1% Os^{4+}, depicted in Fig. 4 is a further proof of the Os^{4+} sensitization. We observe the $\Gamma_5(^1T_{2g})/\Gamma_3(^1E_g)$ excitation bands of Os^{4+}, in addition to the lines characteristic of direct Er^{3+} $^4I_{11/2}$ excitation. The observed quadratic dependence of the $^4S_{3/2}$ upconversion-luminescence intensity on the excitation power at the $\Gamma_5(^1T_{2g})/\Gamma_3(^1E_g)$ excitation energy is a fingerprint of the upconversion process I, and rules out process III.

The excitation spectra in Fig. 4 show a series of intense sharp lines above 11 700 cm^{-1}. Their energetic positions exactly correspond to the ESA $^4I_{13/2}\rightarrow{}^4S_{3/2}$, and consequently we attribute them to process II. The intense $^4S_{3/2}$ upconversion luminescence at the $^4I_{13/2}\rightarrow{}^4S_{3/2}$ ESA energy in Cs_2NaYCl_6:Er^{3+},Os^{4+} crystals is enabled by the initial $\Gamma_5(^1T_{2g})/\Gamma_3(^1E_g)$ absorption of Os^{4+}. The subsequent $a+b$ energy-transfer sequence to $^4I_{13/2}$ is an important step in this upconversion mechanism. It provides a significant population in $^4I_{13/2}$ to enable the $^4I_{13/2}\rightarrow{}^4S_{3/2}$ ESA step.

Efficiency arguments are important in the discussion of sensitization processes. The excitation spectra in Fig. 4 are a measure of the relative efficiencies of the different pathways to induce $^4S_{3/2}$ upconversion luminescence. The middle trace of Fig. 4 indicates that exciting Cs_2NaYCl_6:10% Er^{3+},0.1% Os^{4+} at 10 959 cm^{-1}, corresponding to the Os^{4+} $\Gamma_5(^1T_{2g})/\Gamma_3(^1E_g)$ excitation energy, is almost as efficient as direct $^4I_{11/2}$ excitation below 10 500 cm^{-1}. This is a remarkable result in view of the differences in the concentrations of Er^{3+} and Os^{4+}. It reflects the 100 times higher extinction coefficient of the $\Gamma_5(^1T_{2g})/\Gamma_3(^1E_g)$ absorption of Os^{4+} compared to $^4I_{11/2}$ of Er^{3+} (see Fig. 2), and also implies a high $Os^{4+}\rightarrow Er^{3+}$ energy-transfer efficiency. Despite these favorable characteristics, we cannot take full advantage of the Os^{4+} sensitization potential for Er^{3+} upconversion, because the Cs_2NaYCl_6 host only accepts a maximum Os^{4+} doping concentration of 0.1%. Choosing a host lattice more suitable for the Os^{4+} sensitizer is an obvious way to get around this concentration limitation. All the excitation spectra in Fig. 4 were measured with a narrow-band excitation source ($\approx$1 cm^{-1}), which favors the sharp $^4I_{11/2}$ lines over the rather broad $\Gamma_5(^1T_{2g})/\Gamma_3(^1E_g)$ absorption. Excitation with a broadband source will greatly favor excitation via the Os^{4+} sensitizer.

The efficiency of inducing $^4S_{3/2}$ upconversion luminescence via the Os^{4+} sensitizer is dependent on the Er^{3+} concentration; see the excitation spectra in Fig. 4. This is mainly due to the concentration dependence of process *b* discussed in Sec. IV C 1. As the upconversion process I starts from $^4I_{11/2}$, we find the highest $\Gamma_5(^1T_{2g})/\Gamma_3(^1E_g)$ contribution to the excitation spectrum of the $^4S_{3/2}$ upconversion luminescence in Cs_2NaYCl_6:10% Er^{3+},0.1% Os^{4+}; see Fig. 4.

The relative efficiency of process III is rather independent of the Er^{3+} concentration; see the lines above 11 700 cm^{-1} in the excitation spectra of Fig. 4. This is related to the fact that, independent of the Er^{3+} concentration, a predominant part of the $\Gamma_5(^1T_{2g})/\Gamma_3(^1E_g)$ excitation is transferred to $^4I_{13/2}$.

Not only relative intensities in a given material are important in evaluating the sensitization potential of Os^{4+}; even more important are the relative intensities of the same transition in different materials. As luminescence intensities strongly depend on the exact experimental setup, the error

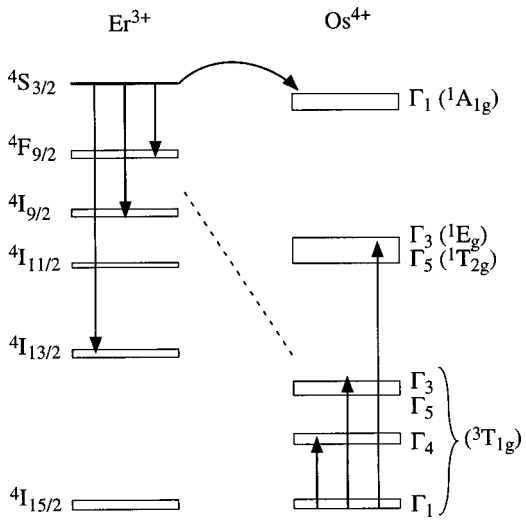

FIG. 11. Energy-transfer processes between Er^{3+} and Os^{4+} involving ${}^4S_{3/2}$. The bent arrow shows the transfer of the whole ${}^4S_{3/2}$ energy to Os^{4+}. Cross-relaxation processes are indicated with pairs of arrows connected by a dashed line.

bars on ratios of luminescence intensities observed in different samples are relatively large. We therefore only give an order of magnitude indication in the following. The ${}^4S_{3/2}$ upconversion-luminescence intensity induced by direct ${}^4I_{11/2}$ excitation at 10 492 cm^{-1} in Cs_2NaYCl_6:10% Er^{3+} is more intense by one order of magnitude than the intensity observed upon the same excitation in the codoped Cs_2NaYCl_6:10% Er^{3+},0.1% Os^{4+}. This intensity reduction is due to the loss processes introduced to the Er^{3+} upconversion system by the presence of Os^{4+}.

In Sec. IV C 1 we have already discussed the losses introduced to ${}^4I_{11/2}$ by the cross-relaxation process *b*. Figure 11 schematically shows the loss processes caused by energy transfer between ${}^4S_{3/2}$ of Er^{3+} and the spin-flip states of Os^{4+}. They involve the transfer of the ${}^4S_{3/2}$ energy to $\Gamma_1({}^1A_{1g})$ and the cross-relaxations ${}^4S_{3/2}+\Gamma_1({}^3T_{1g})\rightarrow{}^4F_{9/2}+\Gamma_4({}^3T_{1g})$, ${}^4S_{3/2}+\Gamma_1({}^3T_{1g})\rightarrow{}^4I_{9/2}+\Gamma_5/\Gamma_3({}^3T_{1g})$, and ${}^4S_{3/2}+\Gamma_1({}^3T_{1g})\rightarrow{}^4I_{13/2}+\Gamma_5({}^1T_{2g})/\Gamma_3({}^1E_g)$. This large number of possible energy-transfer processes is a direct consequence of the rich energy-level structure of the Os^{4+} sensitizer and the Er^{3+} activator with similar energy intervals. The sum of these processes leads to a reduction of the ${}^4S_{3/2}$ lifetime, as documented in Table II. The ${}^4S_{3/2}$ lifetime decreases from 11.2 ms in Cs_2NaYCl_6:2% Er^{3+} to 7.5 ms, 7.2 ms, and 119 μs in Cs_2NaYCl_6:*x*% Er^{3+},0.1% Os^{4+}, with $x=2$, 10, and 100, respectively. This shows that the ${}^4S_{3/2}$ quenching is more important for the samples doped with the higher Er^{3+} concentration, in analogy to the situation described in Sec. IV C 1 for the quenching of ${}^4I_{11/2}$. Finding the optimum concentration of the dopant ions is thus crucial to achieve the most efficient upconversion in the Cs_2NaYCl_6:Er^{3+},Os^{4+} system.

V. CONCLUSIONS

We have analyzed the cooperative processes between Os^{4+} and Er^{3+} in the cubic elpasolite host Cs_2NaYCl_6. Measuring luminescence intensities and lifetimes of the relevant states has revealed the energy-transfer pathways, by which the Os^{4+} excitation is transferred from $\Gamma_5({}^1T_{2g})/\Gamma_3({}^1E_g)$ to ${}^4I_{11/2}$ and ${}^4I_{13/2}$ of Er^{3+}. By transferring the $\Gamma_5({}^1T_{2g})/\Gamma_3({}^1E_g)$ excitation energy to ${}^4I_{11/2}$, Os^{4+} acts as a sensitizer for subsequent Er^{3+} upconversion. The energy transfer to ${}^4I_{13/2}$ opens up the way for an upconversion mechanism at the energy of the ${}^4I_{13/2}\rightarrow{}^4S_{3/2}$ excited-state absorption. Varying concentrations greatly influences the branching between $\Gamma_5({}^1T_{2g})/\Gamma_3({}^1E_g)\rightarrow{}^4I_{11/2}$ and $\Gamma_5({}^1T_{2g})/\Gamma_3({}^1E_g)\rightarrow{}^4I_{13/2}$.

The fact that Er^{3+} upconversion can be sensitized with Os^{4+} at a doping concentration of only 0.1% shows that $5d$ transition-metal ions are promising candidates to sensitize rare-earth upconversion. The sensitization efficiency in the title compound is low, especially for narrow-band laser excitation. Choosing a tetravalent host lattice such as Cs_2ZrCl_6 allowing higher Os^{4+} concentrations and diode-laser excitation should greatly improve the situation. Another problem encountered in the sensitization of Er^{3+} upconversion in the Cs_2NaYCl_6:Er^{3+},Os^{4+} samples is related with the back-transfer of Er^{3+} excitation to Os^{4+}. This occurs in both Er^{3+} states, the intermediate excited state ${}^4I_{11/2}$, and the upper excited state ${}^4S_{3/2}$. By varying the Er^{3+} concentration, the various energy-transfer processes are greatly affected and a tuning of the overall upconversion efficiency is thus achieved.

In addition to sensitizing Er^{3+} upconversion, exciting into the relatively broad $\Gamma_5({}^1T_{2g})/\Gamma_3({}^1E_g)$ states above 10 000 cm^{-1} represents an efficient way to populate ${}^4I_{13/2}$ of Er^{3+}, especially at low Er^{3+} doping concentrations. The ${}^4I_{13/2}\rightarrow{}^4I_{15/2}$ laser transition is of interest for telecommunication applications. These lasers are usually pumped into ${}^4I_{9/2}$ around 12 000 cm^{-1}. The relaxation from ${}^4I_{9/2}$ to the ${}^4I_{13/2}$ upper laser level is based on multiphonon relaxation, which explains why high-phonon energy hosts are desirable for these applications.[33] Pumping samples codoped with Er^{3+} and Os^{4+} into $\Gamma_5({}^1T_{2g})/\Gamma_3({}^1E_g)$ around 11 000 cm^{-1} might represent an alternative route to generate high ${}^4I_{13/2}$ populations in hosts, where the ${}^4I_{11/2}\rightarrow{}^4I_{13/2}$ multiphonon relaxation is inefficient.

ACKNOWLEDGMENTS

This work was financially supported by the Swiss National Science Foundation. We thank O. Wenger and R. Valiente for fruitful discussions, and S. Lüthi for providing the Cs_2NaYCl_6:10% Er^{3+} crystal.

[1] F. E. Auzel, Proc. IEEE **61**, 758 (1973).
[2] B. Jacquier, C. Linares, R. Mahioou, J. L. Adam, E. Denoue, and J. Lucas, J. Lumin. **60-61**, 175 (1997).
[3] R. K. Watts and H. J. Richter, Phys. Rev. B **6**, 1584 (1972).
[4] F. E. Auzel, C. R. Acad. Sci. (Paris) **262**, 1016 (1966).
[5] F. W. Ostermayer, J. P. van der Ziel, H. M. Marcos, L. G. van Uitert, and J. E. Geusic, Phys. Rev. B **3**, 2698 (1971).
[6] P. J. Cresswell, D. J. Robbins, and A. J. Thomson, J. Lumin. **17**, 311 (1978).
[7] M. P. Hehlen, Ph.D. thesis, University of Bern, 1994.
[8] A. D. Kirk, N. Furer, and H. U. Güdel, J. Lumin. **68**, 77 (1996).
[9] C. D. Flint and A. G. Paulusz, Mol. Phys. **41**, 907 (1980).
[10] M. Wermuth and H. U. Güdel, J. Am. Chem. Soc. **121**, 10102 (1999).
[11] M. Wermuth and H. U. Güdel, J. Chem. Phys. **114**, 1393 (2001).
[12] T. L. Brown, W. G. McDugle, and L. G. Kent, J. Am. Chem. Soc. **92**, 3645 (1970).
[13] J. B. Reed, B. S. Hopkins, and L. F. Audrieth, Inorg. Synth. **1**, 28 (1978).
[14] G. Meyer, Inorg. Synth. **25**, 146 (1989).
[15] G. H. Dieke, in *Spectra and Energy Levels of Rare Earth Ions in Crystals*, edited by H. M. Crosswhite and H. Crosswhite (Wiley, New York, 1968).
[16] S. M. Khan, H. H. Patterson, and H. Engstrom, Mol. Phys. **35**, 1623 (1978).
[17] W. H. Inskeep, R. W. Schwartz, and P. N. Schatz, Mol. Phys. **25**, 805 (1973).
[18] S. B. Piepho, J. R. Dickinson, J. A. Spencer, and P. N. Schatz, Mol. Phys. **24**, 609 (1972).
[19] L. C. Weiss, P. J. McCarthy, J. P. Jasinski, and P. N. Schatz, Inorg. Chem. **17**, 2689 (1978).
[20] M. Wermuth, C. Reber, and H. U. Güdel, Inorg. Chem. (to be published).
[21] B. A. Kozikowski and T. A. Keiderlin, Mol. Phys. **40**, 477 (1980).
[22] S. C. Weaver and D. S. McClure, Inorg. Chem. **31**, 2814 (1992).
[23] D. H. Brown, K. R. Dixon, C. M. Livingston, R. H. Nuttall, and D. W. A. Sharp, J. Chem. Soc. A 100 (1967).
[24] K. W. Fung and K. E. Johnson, Inorg. Chem. **10**, 1347 (1971).
[25] I. Sun, E. H. Ward, and C. L. Hussey, J. Electrochem. Soc. **135**, 3035 (1988).
[26] M. Bruns and W. Preetz, Z. Anorg. Allg. Chem. **537**, 88 (1986).
[27] H. H. Schmidtke, H. Lehnert, and M. Giesbers, Spectrochim. Acta, Part A **53**, 789 (1997).
[28] B. A. Kozikowski and T. A. Keiderling, J. Phys. Chem. **87**, 4630 (1983).
[29] F. S. Richardson, M. F. Reid, J. J. Dallara, and R. D. Smith, J. Chem. Phys. **83**, 3813 (1985).
[30] S. R. Lüthi, M. Pollnau, H. U. Güdel, and M. P. Hehlen, Phys. Rev. B **60**, 162 (1999).
[31] S. Lüthi, Diploma thesis, University of Bern, 1994.
[32] Z. Hasan, L. Biyikli, M. J. Sellars, G. A. Khodaparast, F. S. Richardson, and J. R. Quagliano, Phys. Rev. B **56**, 4518 (1997).
[33] T. Schweizer, T. Jensen, E. Heumann, and G. Huber, Opt. Commun. **118**, 557 (1995).